

AFUNet: Cross-Iterative Alignment-Fusion Synergy for HDR Reconstruction via Deep Unfolding Paradigm

Xinyue Li¹, Zhangkai Ni^{1*}, Wenhan Yang²

¹Tongji University, ²Pengcheng Laboratory

2252065@tongji.edu.cn, zkni@tongji.edu.cn, yangwh@pcl.ac.cn

Abstract

Existing learning-based methods effectively reconstruct HDR images from multi-exposure LDR inputs with extended dynamic range and improved detail, but they rely more on empirical design rather than theoretical foundation, which can impact their reliability. To address these limitations, we propose the cross-iterative Alignment and Fusion deep Unfolding Network (AFUNet), where HDR reconstruction is systematically decoupled into two interleaved subtasks—alignment and fusion—optimized through alternating refinement, achieving synergy between the two subtasks to enhance the overall performance. Our method formulates multi-exposure HDR reconstruction from a Maximum A Posteriori (MAP) estimation perspective, explicitly incorporating spatial correspondence priors across LDR images and naturally bridging the alignment and fusion subproblems through joint constraints. Building on the mathematical foundation, we reimagine traditional iterative optimization through unfolding—transforming the conventional solution process into an end-to-end trainable AFUNet with carefully designed modules that work progressively. Specifically, each iteration of AFUNet incorporates an Alignment-Fusion Module (AFM) that alternates between a Spatial Alignment Module (SAM) for alignment and a Channel Fusion Module (CFM) for adaptive feature fusion, progressively bridging misaligned content and exposure discrepancies. Extensive qualitative and quantitative evaluations demonstrate AFUNet’s superior performance, consistently surpassing state-of-the-art methods. Our code is available at: <https://github.com/eezkni/AFUNet>

1. Introduction

Multi-exposure High Dynamic Range (HDR) imaging aims to effectively leverage information from multiple Low Dynamic Range (LDR) images captured at varying exposures to reconstruct a larger dynamic range HDR image [5]. HDR

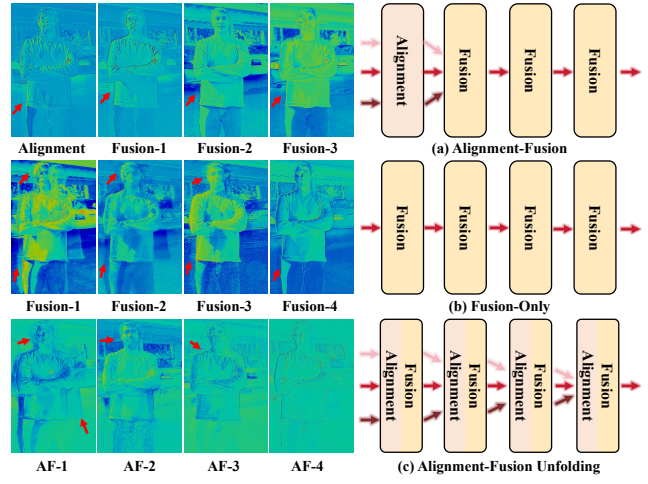


Figure 1. Comparison of three HDR reconstruction paradigms: (a) the “Alignment-Fusion” paradigm, (b) the “Fusion-Only” paradigm, and (c) our proposed “Alignment and Fusion Unfolding” paradigm. The feature maps from the reconstruction process of the three paradigms are shown on the left. (c) shows superior deghosting due to iterative alignment that continuously corrects misalignment, while (a) leaves artifacts due to pre-alignment, and (b) lacks explicit alignment, resulting in less effective deghosting.

images possess a broader dynamic range, offering a realistic and visually appealing experience, making it indispensable for applications such as satellite remote sensing, virtual reality and autonomous driving.

While existing HDR methods can produce accurate results when LDR images are well-aligned [5, 22, 28, 47], misalignment issues caused by dynamic scenes or camera jitter are prone to induce ghosting artifacts. Traditional methods make effort in either rejecting misaligned pixels [7, 27, 47], merging images at the patch level [10, 16, 21, 29], or performing explicit alignment of LDR images [1, 14, 50]. However, these methods are still far from being practical. Rejection-based methods might miss important details in moving regions, patch-based methods are computationally intensive, while alignment-based methods heavily depend on precise alignment, which is challenging under large mo-

*Corresponding author.

tion or poor exposure conditions.

With the rise of deep learning-based methods, leveraging data priors and flexible modeling has allowed more effective solutions to these challenges. They generally follow two main paradigms, as shown in Fig. 1. The majority of methods [4, 18, 39, 41, 48] adopt a two-stage paradigm: first utilizing an alignment module to align LDR images and then refine through a complex network to fuse features and reconstruct the HDR image, which is referred to as the “Alignment-Fusion” paradigm. In contrast, the other branch [33, 40, 44] bypasses alignment, instead directly fusing features implicitly through stacked modules, summarized as the “Fusion-Only” paradigm. While both paradigms have proven effective, the former often loses information during the alignment process, while the latter lacks explicit alignment, leading to ghosting. Additionally, both paradigms lack mathematical foundation and are designed empirically. To address these issues, we propose a novel approach that performs alignment and fusion alternately. We formulate HDR imaging from the MAP view and translate this formulation into an end-to-end trainable network through unfolding the iterative optimization steps.

In this study, we propose a cross-iterative alignment and fusion deep unfolding network, achieving superior performance. Our key insight is to decouple the complex HDR reconstruction process into alignment and fusion subproblems with two prior regularization terms to capture the spatial correspondence among multi-exposure LDR images. Then we turn the iterative reconstruction steps into a fixed number of designed concatenated blocks. Unlike prior deep unfolding methods that take HDR imaging as a low-rank completion problem [23], our method is more flexible and relaxed, accommodating more real-world scenarios without relying on additional or strict assumptions. Furthermore, unlike MERF [9], which uses a GAN-like iterative training strategy, ours is simple and requires no separate pre-training stage. The main contributions are as follows:

- **A Unified MAP View for HDR Reconstruction:** We formulate HDR reconstruction as a Maximum A Posteriori (MAP) estimation problem, introducing prior regularization terms that constrain the spatial correspondence among LDRs to decompose the task into alignment and fusion subproblems, which are solved in an cross-iterative manner for achieving high-quality results.
- **End-to-End Theory-Grounded Unfolding Network:** We develop a cross-iterative Alignment and Fusion deep Unfolding Network (**AFUNet**) that allows end-to-end training for HDR reconstruction. AFUNet is meticulously designed, grounded in mathematical theory, and comprises stacked Alignment Fusion Modules (AFMs) corresponding to iterative stages.
- **State-of-the-Art Performance:** Extensive qualitative and quantitative experiments demonstrate that AFUNet

achieves state-of-the-art performance in HDR reconstruction, delivering visually appealing results that align with human perceptual aesthetics.

2. Related Work

2.1. Learning-based HDR Reconstruction Methods

Most existing deep learning-based HDR reconstruction methods follow the “Alignment-Fusion” paradigm. Early non-end-to-end methods [13] first align LDR images using optical flow before fusing them to produce HDR images. Although Kalantari *et al.* [13] shows notable improvements over traditional approaches, it remains error-prone in handling complex foreground motions. Subsequent techniques improve alignment through advanced motion estimation modules [2, 15] or by employing attention-based feature alignment within Convolutional Neural Network (CNN) frameworks [18, 39]. More recently, transformer-based methods [20, 32, 41] leveraged multi-head self-attention mechanisms for enhanced alignment and fusion capabilities. Additionally, some methods [33, 40, 44] bypass the alignment, performing only feature fusion. While these paradigms achieve promising performance, their deep neural network architectures often function as black boxes, with empirically designed structures. Deep Unfolding Networks (DUNs) have gained traction for HDR tasks, balancing the advantages of model-based and learning-based approaches while addressing their limitations. In this work, we introduce a novel deep unfolding paradigm that combines the strengths of the “Alignment-Fusion” paradigm with model-based techniques, resulting in a theoretically informed end-to-end trainable network.

2.2. Deep Unfolding Networks

DUNs have shown strong performance on inverse problems like Super-Resolution [12, 46, 49], Compressive Sensing [8, 31, 35], and Pan-Sharpening [25, 36, 43] by unfolding model-based iterative algorithms into end-to-end optimized deep networks. However, DUNs are relatively underexplored in the multi-exposure HDR imaging field. Mai *et al.* [23] applied an unrolling strategy for HDR imaging, modeling it through low-rank tensor completion to construct an interpretable deep network. Though Mai *et al.* [23] is effective in some cases, it is limited in HDR reconstruction because its low-rank modeling oversimplifies complex scenes, misses crucial details, and does not fully utilize available information. In contrast, our method proposes a simpler but effective model that fully leverages multi-exposure information and provides a more general solution for multi-exposure HDR imaging. Our carefully designed, explainable deep unfolding approach achieves both qualitative and quantitative improvements, delivering state-of-the-art HDR reconstruction results.

3. Methodology

3.1. Motivation

Given a set of LDR multi-exposure images, we aim to address the following two issues:

- **Limited Deghosting Effectiveness.** The “Alignment-Fusion” paradigm, based on pre-alignment, struggles with LDRs due to motion-induced misalignments and information loss in over- or under-exposed regions, which hinder precise alignment. While pre-alignment has shown some efficacy, relying solely on this strategy is less than ideal for HDR reconstruction. Integrating alignment directly into the fusion process holds the promise of more effectively suppressing ghosting artifacts.
- **Lack of Mathematical Foundation.** Deep learning has propelled significant advances in HDR reconstruction, but various prevailing architectures lack mathematical foundation, often being empirically constructed. Moreover, the absence of a theoretical foundation often results in redundant model parameters, ultimately hindering further performance enhancements.

Our core goal is to develop a well-structured model specifically tailored for HDR reconstruction that effectively aligns and fuses multi-exposure images progressively to produce high-quality HDR outputs. In the following sections, we introduce our proposed method in detail.

3.2. Problem Formulation

The degradation process from an HDR image to an LDR image can be mathematically formulated as $y = Dx + n$, where x denotes the HDR image, D represents the degradation transformation, y is the LDR image, and n is the additive noise. The intractable ill-posed problem of reconstructing x is reformulated as an optimization problem under the MAP framework, including data fidelity and regularization terms $\Psi(\cdot)$. The data fidelity term is typically defined as the ℓ_2 norm, expressed in the following energy function:

$$\hat{x} = \arg \min_x \frac{1}{2} \|y - Dx\|_2^2 + \lambda \Psi(x), \quad (1)$$

where \hat{x} is the reconstructed HDR image, λ is a regularization weighting hyperparameter. We aim to merge three differently exposed LDR images (*i.e.*, under-exposed image y_1 , normal-exposed image y_2 , and over-exposed image y_3) into a single high-quality HDR image \hat{x} without artifacts. Specifically, the LDR image y_2 serves as the reference image, and the predicted HDR image must be content-aligned with y_2 . Accordingly, we extend Eq. (1) by introducing the non-reference LDR images y_1 and y_3 , which provide complementary scene details from their distinct exposure levels and thereby enhance the reconstruction of x from y_2 .

However, directly applying the priors from the non-reference LDR images might limit their effective utilization due to potential misalignment between the LDR images. To address this issue, we introduce two spatial correspondence prior regularization terms, $p_1(y_2, \alpha_1)$ and $p_3(y_2, \alpha_3)$, which explicitly model the rich priors between the non-reference LDR images y_1, y_3 and the reference LDR image y_2 for HDR reconstruction. The α_1 and α_3 represent the spatially aligned versions of y_1 and y_3 , respectively, which are iteratively optimized to align the structure and content with x . Thus, we reformulate the optimization problem for HDR reconstruction as follows:

$$\arg \min_{x, \alpha_1, \alpha_3} \|y_2 - D_2 x\|_2^2 + \lambda_1 p_1(D_1 x, \alpha_1) + \lambda_3 p_3(D_3 x, \alpha_3), \quad (2)$$

where λ_1, λ_3 are balancing coefficients, and D_1, D_3 are the degradation transformations of y_1, y_3 , respectively.

To solve this model efficiently, we first decompose Eq. (2) into two subproblems—alignment and fusion—and solve them alternately:

$$\alpha_1^t = \arg \min_{\alpha_1} p_1(D_1 x^{t-1}, \alpha_1), \quad (3a)$$

$$\alpha_3^t = \arg \min_{\alpha_3} p_3(D_3 x^{t-1}, \alpha_3), \quad (3b)$$

$$x^t = \arg \min_x \frac{1}{2} \|y_2 - D_2 x\|_2^2 + \lambda_1 p_1(D_1 x, \alpha_1^t) + \lambda_3 p_3(D_3 x, \alpha_3^t). \quad (3c)$$

For the alignment subproblem in Eq. (3a) and Eq. (3b), we define gradient descent operators $G_i(\cdot) = \alpha_i^{t-1} - \varsigma_i \nabla_{\alpha_i} p_i(D_i x^{t-1}, \alpha_i^{t-1})$, where ς_i is the step size, $\nabla_{\alpha_i} p_i(D_i x^{t-1}, \alpha_i^{t-1})$ are the gradient of the spatial correspondence prior term for the aligned variables α_i , $i = 1, 3$. The t -th optimization step can be expressed as:

$$\alpha_1^t = G_1(\alpha_1^{t-1}), \quad (4a)$$

$$\alpha_3^t = G_3(\alpha_3^{t-1}). \quad (4b)$$

For the fusion subproblem in Eq. (3c), we solve it using the Half Quadratic Splitting (HQS) [6] method to decouple the data fidelity term and regularization terms. First, we introduce two auxiliary variables, u and v , corresponding to the two prior regularization terms that constrain the spatial correspondence among different LDR images. We impose constraints to ensure that u and v are as close as possible to the target image x :

$$\begin{aligned} & \arg \min_{x, u, v} \frac{1}{2} \|y_2 - D_2 x\|_2^2 + \lambda_1 p_1(D_1 u, \alpha_1^t) \\ & + \lambda_3 p_3(D_3 v, \alpha_3^t) + \frac{\beta_1}{2} \|u - x\|_2^2 + \frac{\beta_3}{2} \|v - x\|_2^2, \end{aligned} \quad (5)$$

where β_1 and β_3 are weighting factors for the added terms.

The fusion problem can then be split into three subproblems, which are updated iteratively:

$$u^t = \arg \min_u \frac{\beta_1}{2} \|u - x^{t-1}\|_2^2 + \lambda_1 p_1(D_1 u, \alpha_1^t), \quad (6a)$$

$$v^t = \arg \min_v \frac{\beta_3}{2} \|v - x^{t-1}\|_2^2 + \lambda_3 p_3(D_3 v, \alpha_3^t), \quad (6b)$$

$$x^t = \arg \min_x \frac{1}{2} \|y_2 - D_2 x\|_2^2 + \frac{\beta_1}{2} \|u^t - x\|_2^2 + \frac{\beta_3}{2} \|v^t - x\|_2^2. \quad (6c)$$

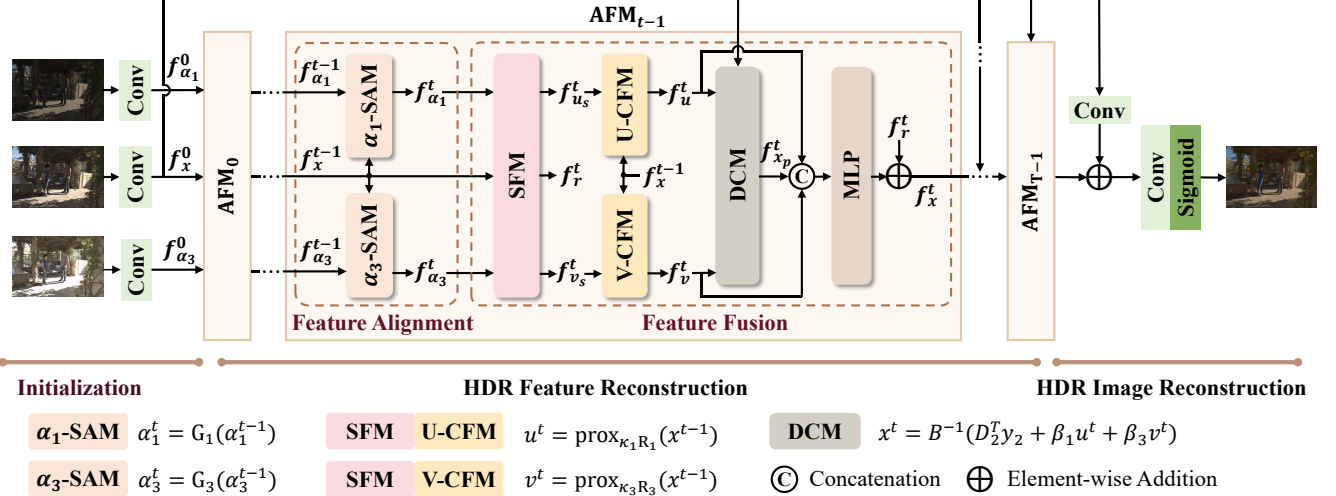


Figure 2. Framework of the AFUNet for HDR reconstruction consists of three main processes: Initialization, HDR Feature Reconstruction, and HDR Image Reconstruction. Within HDR Feature Reconstruction, stacked Alignment Fusion Modules (AFMs) iteratively refine target HDR features via alternating alignment and fusion. In the Feature Alignment subprocess, $f_{\alpha_1}^{t-1}$ and $f_{\alpha_3}^{t-1}$ are aligned with f_x^{t-1} by the Spatial Alignment Modules—denoted as $\alpha_1\text{-SAM}$ and $\alpha_3\text{-SAM}$. In the Feature Fusion subprocess, the Spatial Fusion Module (SFM) performs preliminary optimization to obtain $f_{u_s}^t$ and $f_{v_s}^t$, followed by the Channel Fusion Modules—denoted as U-CFM and V-CFM—obtain f_u^t and f_v^t , respectively. Finally, the Data Consistency Module (DCM) obtains $f_{x_p}^t$, and an MLP with residual addition further refines f_x^t before it is transmitted to the next stage. The $\kappa_i = \frac{\lambda_i}{\beta_i}$, $R_i = p_i(\cdot, \alpha_i^t)$ ($i = 1, 3$), and $B^{-1} = (D_2^T D_2 + (\beta_1 + \beta_3)I)^{-1}$.

Given reconstruction target image x^{t-1} and aligned image α_1^t and α_3^t , we define proximal operators $\text{prox}_{\frac{\lambda_1}{\beta_1} P_1}(\cdot)$ and $\text{prox}_{\frac{\lambda_3}{\beta_3} P_3}(\cdot)$ for the optimization of u^t and v^t : $\text{prox}_{\frac{\lambda_1}{\beta_1} P_1}(\cdot, \alpha_1^t) = \arg \min_u \frac{\beta_1}{2} \|u - x^{t-1}\|_2^2 + \lambda_1 P_1(D_1 u, \alpha_1^t)$ and $\text{prox}_{\frac{\lambda_3}{\beta_3} P_3}(\cdot, \alpha_3^t) = \arg \min_v \frac{\beta_3}{2} \|v - x^{t-1}\|_2^2 + \lambda_3 P_3(D_3 v, \alpha_3^t)$. Eq. (6a) and Eq. (6b) is then solved by the following equation:

$$u^t = \text{prox}_{\frac{\lambda_1}{\beta_1} P_1}(\cdot, \alpha_1^t)(x^{t-1}), \quad (7a)$$

$$v^t = \text{prox}_{\frac{\lambda_3}{\beta_3} P_3}(\cdot, \alpha_3^t)(x^{t-1}). \quad (7b)$$

Eq. (6c) represents a quadratic regularized least squares problem, which has a closed-form solution:

$$x^t = (D_2^T D_2 + (\beta_1 + \beta_3)I)^{-1}(D_2^T y_2 + \beta_1 u^t + \beta_3 v^t), \quad (8)$$

where I is the identity matrix, D_2^T designates the transposition of degradation transformation matrix D_2 . The matrix inverse is computationally expensive, so we treat $(D_2^T D_2 + (\beta_1 + \beta_3)I)^{-1}$ as a single entity, denoted as B^{-1} . To efficiently handle this, we design neural networks to learn the complex degradation matrices B^{-1} and D_2^T .

3.3. Deep Unfolding Network

The AFUNet pipeline, as illustrated in Fig. 2, consists of three primary processes: **Initialization**, **HDR Feature Reconstruction**, and **HDR Image Reconstruction**. The feature reconstruction process includes T stages for optimiza-

tion. Each stage can be further subdivided into two key subprocesses: **Feature Alignment** and **Feature Fusion**. Notably, as outlined in Section 3.2, the solution to the unfolding paradigm is performed in the image space, where the LDR images y_1, y_2, y_3 are directly involved in the optimization process. In contrast, in this section, we apply the iterative optimization and refinement at the feature space and propose a learnable solution using a deep unfolding network. *The algorithm of AFUNet is available in Section 2 of the supplementary material.* The details are as follows:

1) Initialization. Given the input images $y_i = [L_i, H_i] \in \mathbb{R}^{B \times 6 \times H \times W}$ ($i = 1, 2, 3$), where L_i is the LDR image and H_i refers to the gamma-corrected result of L_i that provides additional information, these images are projected into the feature domain $f_{y_i} \in \mathbb{R}^{B \times C \times H \times W}$ ($i = 1, 2, 3$) through three shallow feature extraction modules $\text{SFEM}_i(\cdot)$, respectively. B, C, H , and W denote the batch size, number of channels, height, and width of the feature maps, respectively. The feature extraction is expressed as:

$$f_{y_i} = \text{SFEM}_i(y_i), \quad i = 1, 2, 3, \quad (9)$$

where $\text{SFEM}_i(\cdot)$ is a convolutional layer with a 3×3 kernel. The feature maps $f_{y_1}, f_{y_2}, f_{y_3}$ are used to initialize the features $f_{\alpha_1}^0, f_x^0, f_{\alpha_3}^0$, respectively, which serve as the initial input features for the HDR feature reconstruction process.

2) HDR Feature Reconstruction. We propose T stages using the stacked Alignment Fusion Modules (AFMs), which are unfolded from our iterative optimization algorithms to solve the HDR reconstruction objective. Impor-

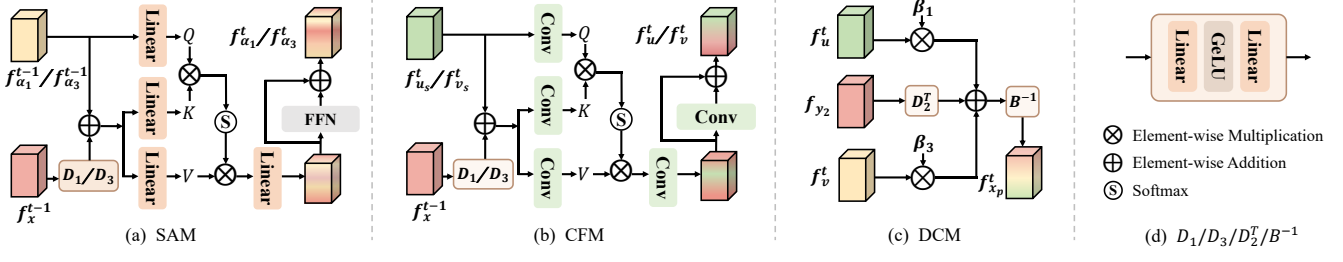


Figure 3. (a) SAM uses window-based cross-attention to align $f_{\alpha_1}^{t-1}$ or $f_{\alpha_3}^{t-1}$ with f_x^t , to obtain $f_{\alpha_1}^t$ or $f_{\alpha_3}^t$. (b) CFM fuses $f_{u_s}^t$ or $f_{v_s}^t$ with f_x^{t-1} , to obtain f_u^t or f_v^t . (c) DCM updates f_x^t to obtain $f_{x_p}^t$ using f_u^t , f_v^t . (d) The degradation transformations, including D_1 , D_3 , D_2^T , and B^{-1} , are learned using independent MLPs.

tantly, all stages share the same structure but have independent parameters. The iterative process is expressed as:

$$f_{\alpha_1}^t, f_x^t, f_{\alpha_3}^t = \text{AFM}_{t-1}(f_{\alpha_1}^{t-1}, f_x^{t-1}, f_{\alpha_3}^{t-1}), \quad (10)$$

where $t = 1, 2, \dots, T$. The features $f_{\alpha_1}^{t-1}, f_x^{t-1}, f_{\alpha_3}^{t-1}$ represent the outputs from stage $t - 2$, i.e., the previous stage, and $f_{\alpha_1}^t, f_x^t, f_{\alpha_3}^t$ are the outputs from stage $t - 1$.

A. Feature Alignment Subproblem. We design a simple but effective Spatial Alignment Module (SAM) to align $f_{\alpha_1}^{t-1}, f_{\alpha_3}^{t-1}$ with the intermediate reconstructed feature f_x^{t-1} . There are two SAMs act as gradient descent operators $G_1(\cdot)$ and $G_3(\cdot)$ in Eq. (4a) and (4b), respectively, producing the aligned features $f_{\alpha_1}^t, f_{\alpha_3}^t$. As shown in Fig. 3 (a), we construct the SAM as a window-based cross-attention transformer block [19], which can be formulated as:

$$f_{\alpha_i}^t = \text{FFN}(\text{WCAA}(f_{\alpha_i}^{t-1}, f_x^{t-1})), \quad (11)$$

where WCAA(\cdot) is the Window-based Cross-Attention Alignment module, and FFN(\cdot) is a Feed-Forward Network, with $i = 1, 3$. This enables us to query the spatial information in the reference image feature and use f_x^{t-1} to preserve the spatial structure of the reference image.

$$\text{WCAA}(f_{\alpha_i}^{t-1}, f_x^{t-1}) = \text{Softmax}\left(\frac{QK^T}{\sqrt{d_k}}\right)V, \quad (12)$$

where

$$\begin{aligned} Q &= \text{W}_Q(f_{\alpha_i}^{t-1}), \\ K &= \text{W}_K(f_{\alpha_i}^{t-1} + \text{MLP}_{D_i}(f_x^{t-1})), \\ V &= \text{W}_V(f_{\alpha_i}^{t-1} + \text{MLP}_{D_i}(f_x^{t-1})), \end{aligned}$$

$\text{W}_Q(\cdot), \text{W}_K(\cdot)$ and $\text{W}_V(\cdot)$ are learnable transformations, d_k is the feature channel dimension of Q and K , $\text{MLP}_{D_i}(\cdot)$ denotes $\text{MLP}(\cdot)$ for learning degradation transformations D_i ($i = 1, 3$) as shown in Fig. 3 (d). Notably, we use window-based cross-attention to focus on local spatial information between features, as alignment primarily targets high-frequency and structural details. In contrast, global transformations, such as warping, lead to suboptimal alignment results due to their application of uniform transformations across the entire image.

B. Feature Fusion Subproblem. It involves the updating of three variables: f_u^t , f_v^t , and f_x^t .

Update f_u^t and f_v^t : For the optimization of f_u^t and f_v^t according to Eq. (7a) and Eq. (7b), we propose a two-step fusion module as the proximal operator for learning priors between features. First, it fuses features spatially and then conducts channel-wise fusion to integrate f_x^{t-1} with $f_{\alpha_1}^t$ and $f_{\alpha_3}^t$. This process can be expressed as:

$$f_{u_s}^t, f_r^t, f_{v_s}^t = \text{SFM}(f_{\alpha_1}^t, f_x^{t-1}, f_{\alpha_3}^t), \quad (13a)$$

$$f_u^t = \text{U-CFM}(f_{u_s}^t, f_x^{t-1}), \quad (13b)$$

$$f_v^t = \text{V-CFM}(f_{v_s}^t, f_x^{t-1}). \quad (13c)$$

1) Spatial Fusion Module. The SFM(\cdot) is a Transformer-based Spatial Fusion Module where $f_{\alpha_1}^t$, f_x^{t-1} , and $f_{\alpha_3}^t$ are concatenated as inputs, producing an output split into $f_{u_s}^t$, f_r^t and $f_{v_s}^t$, where f_r^t denotes the residual feature.

2) Channel Fusion Module. As illustrated in Fig. 3 (b), the U-CFM(\cdot) and V-CFM(\cdot) are channel attention-based Transformers [45] that refine the interaction between f_x^{t-1} and the spatially fused outputs $f_{u_s}^t$ or $f_{v_s}^t$ to update f_u^t and f_v^t , respectively, while f_x^{t-1} remains unchanged based on our formulation.

Update f_x^t : As illustrated in Fig. 3 (c), for the optimization of variable f_x^{t-1} from the previous stage, utilizing the updated results f_u^t and f_v^t from Eq. (13b) and Eq. (13c), we proceed through the Data Consistency Module DCM(\cdot) to obtain $f_{x_p}^t$ according to Eq. (8), as expressed in the following equation:

$$f_{x_p}^t = \text{DCM}(f_u^t, f_{y_2}, f_v^t), \quad (14)$$

where $f_{x_p}^t$ refers to the preliminary update result of f_x^{t-1} . Then, we fuse optimized variables $f_u^t, f_{x_p}^t, f_v^t$ and do dimension reduction using $\text{MLP}(\cdot)$ to further update $f_{x_p}^t$. Subsequently, we add the residual feature f_r^t to obtain f_x^t .

$$f_x^t = \text{MLP}([f_u^t, f_{x_p}^t, f_v^t]) + f_r^t. \quad (15)$$

Finally, we transmit optimized variables, $f_{\alpha_1}^t$, f_x^t , and $f_{\alpha_3}^t$ to the next stage.

3) HDR Image Reconstruction. After completing all the unfolding reconstruction stages, we obtain the final reconstructed HDR feature f_x^T . To ensure stability in HDR

image reconstruction, we employ a residual strategy and then project the feature into the reconstructed HDR image \hat{x} . The reconstruction process is defined as follows:

$$\hat{x} = \text{Sigmoid}(\text{Conv}(f_x^T + \text{Conv}(f_{y_2}))), \quad (16)$$

where $\text{Sigmoid}(\cdot)$ and $\text{Conv}(\cdot)$ represent the Sigmoid activation function and convolutional operation, respectively.

3.4. Training Loss

Our model is trained end-to-end with the linear combination of \mathcal{L}_1 loss and perceptual loss \mathcal{L}_p . Considering that computing the loss in the HDR domain leads to less effective training [13], we calculate the loss in the tone-mapped domain by applying the μ -law function, the total loss \mathcal{L} is:

$$\mathcal{L} = \|\tau(x) - \tau(\hat{x})\|_1 + \eta \sum_k \|\phi_k(\tau(x)) - \phi_k(\tau(\hat{x}))\|_1, \quad (17)$$

where $\tau(x) = \frac{\log(1+\mu x)}{\log(1+\mu)}$ is the tone-mapping function with $\mu = 5000$. $\phi_k(\cdot)$ is the feature from the k -th layer of the VGG-19 [30], and $\eta = 0.005$ is the weighting parameter.

4. Experiments

This section validates the performance of AFUNet through extensive quantitative and qualitative comparisons, along with ablation studies. *Additional quantitative comparisons, qualitative results, and detailed ablation studies are included in the supplementary material.*

4.1. Experimental Setups

Dataset. All methods are trained using three publicly available and widely used datasets, employing the same training settings: Kalantari’s dataset [13], which consists of 74 samples for training and 15 for testing, Tel’s dataset [33], which contains 108 training samples and 36 testing samples, Hu’s dataset [10] with 85 samples for training and 15 samples for testing. Moreover, to further validate the model’s generalizability, we test on Tursun’s dataset [34] only for qualitative assessment, which lacks ground truth.

Evaluation Metrics. We use peak signal-to-noise ratio (PSNR) and SSIM [37] as evaluation metrics, calculating both metrics in the linear and tone-mapped domains, denoted as ‘-l’ and ‘- μ ’, respectively. Moreover, we adopt HDR-VDP2 [24] that measures the human visual difference between results and targets.

Implementation Details. Our implementation is in PyTorch, and the AFUNet model is configured with a default of 4 stages. Each stage is comprised of 2 SAMs, 1 SFM, and 2 CFMs. During training, we sample 128×128 patches from the dataset and apply data augmentation techniques including random cropping, rotation, and flipping. We use the Adam optimizer with a batch size of 6 and an initial learning

Method	PSNR- μ	PSNR-l	SSIM- μ	SSIM-l	HDR-VDP2
DHDR	41.64	40.91	0.9869	0.9858	60.50
AHDR	43.62	41.03	0.9900	0.9862	62.30
NHDRR	42.41	41.08	0.9887	0.9861	61.21
HDR-GAN	43.92	41.57	0.9905	0.9865	65.45
ADNet	44.37	41.88	0.9917	0.9892	66.02
APNT	43.94	41.61	0.9898	0.9879	64.05
FlexHDR	44.35	42.60	0.9931	0.9902	66.56
CA-ViT	44.32	42.18	0.9916	0.9884	66.03
HyHDR	44.64	42.47	0.9915	0.9894	66.05
DiffHDR	44.11	41.73	0.9911	0.9885	65.52
SCTNet	44.43	42.21	0.9918	0.9891	66.64
LFDiff	44.76	42.59	0.9919	0.9906	66.54
SAFNet	44.66	43.18	0.9919	0.9901	66.69
RFG-HDR	44.21	42.16	0.9915	0.9893	66.47
Ours	44.91	42.59	0.9923	0.9906	66.75

Table 1. Quantitative comparisons on Kalantari’s dataset [13]. The top three performances are highlighted in red, orange, and yellow backgrounds, respectively.

Method	PSNR- μ	PSNR-l	SSIM- μ	SSIM-l	HDR-VDP2
DHDR	41.13	41.20	0.9870	0.9941	70.82
AHDR	45.76	49.22	0.9956	0.9980	75.04
NHDRR	45.15	48.75	0.9956	0.9981	74.86
HDR-GAN	45.86	49.14	0.9945	0.9989	75.19
APNT	46.41	47.97	0.9953	0.9986	73.06
CA-ViT	48.10	51.17	0.9947	0.9989	77.12
HyHDR	48.46	51.91	0.9959	0.9991	77.24
DiffHDR	48.03	50.23	0.9954	0.9989	76.22
SCTNet	48.10	51.14	0.9963	0.9991	77.14
LFDiff	48.74	52.10	0.9968	0.9993	77.35
Ours	48.83	52.13	0.9968	0.9991	77.44

Table 2. Quantitative comparisons on Hu’s dataset [10].

rate of 5×10^{-4} , which is decayed to 5×10^{-6} using cosine decay. The model is trained for 400 epochs on a single NVIDIA GeForce 4090 GPU.

4.2. Comparison with the State-of-the-art Methods

To comprehensively evaluate our model, we compare it with several conventional and state-of-the-art methods from various categories. These include CNN-based methods, *i.e.*, DHDR [38], AHDR [39], NHDRR [40], ADNet [18], APNT [3], FlexHDR [2] and SAFNet [15]; Generative Adversarial Network (GAN)-based methods, *i.e.*, HDR-GAN [26]; Transformer-based methods, *i.e.*, CA-ViT [20], HyHDR [41], SCTNet [33] and RFG-HDR [17]; Diffusion model-based methods, *i.e.*, DiffHDR [42] and LFDiff [11].

Qualitative Comparison. The quantitative results of AFUNet on three widely-used datasets, *i.e.* Kalantari’s dataset [13], Hu’s dataset [10], and Tel’s dataset [33], are presented in Tab. 1, Tab. 2 and Tab. 3, respectively. Our method is compared with classical and state-of-the-art approaches, which include challenging scenarios such as

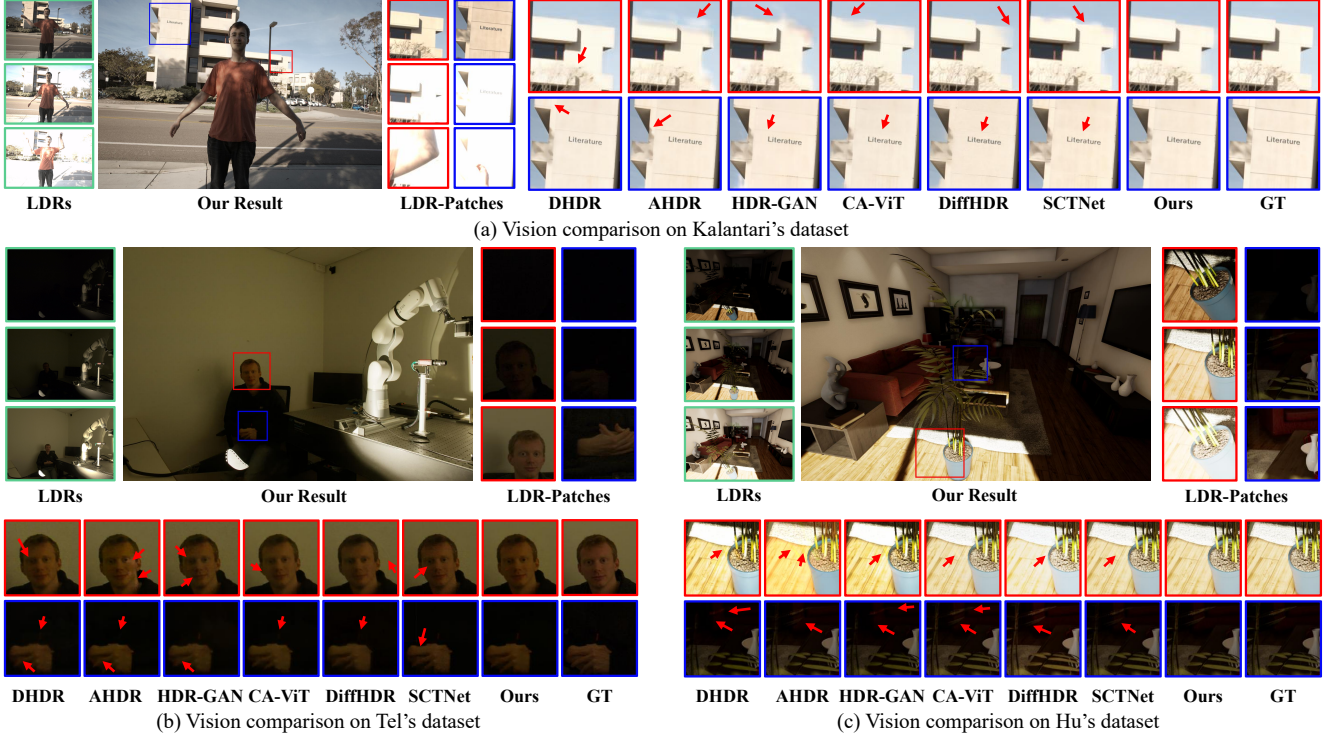


Figure 4. Qualitative comparison between our method and state-of-the-art methods on three datasets: (a) Kalantari’s dataset [13], (b) Tel’s dataset [33], and (c) Hu’s dataset [10].

Method	PSNR- μ	PSNR- l	SSIM- μ	SSIM- l	HDR-VDP2
DHDR	40.05	43.37	0.9794	0.9924	67.09
AHDR	42.08	45.30	0.9837	0.9943	68.80
NHDDR	36.68	39.61	0.9590	0.9853	65.41
HDR-GAN	41.71	44.87	0.9832	0.9949	69.57
CA-ViT	42.39	46.35	0.9844	0.9948	69.23
DiffHDR	42.18	45.63	0.9841	0.9946	69.88
SCTNet	42.55	47.51	0.9850	0.9952	70.66
Ours	43.31	47.83	0.9876	0.9959	71.08

Table 3. Quantitative comparisons on Tel’s dataset [33].

under/over-exposure regions and large misalignment, which are prone to causing ghosting artifacts. Notably, AFUNet exhibits great improvement over previous methods, surpassing Transformer-based methods CA-ViT [20] and SCTNet [33] by 0.59 dB and 0.48 dB in PSNR- μ , 0.41 dB and 0.38 dB in PSNR- l , respectively, on Kalantari’s dataset. In addition, AFUNet outperforms the other leading methods, achieving better reconstruction performance. Compared to LFIDiff [11], AFUNet demonstrates improvements of 0.14 dB and 0.04 dB in PSNR- μ and SSIM- μ on Kalantari’s dataset. Furthermore, it surpasses SAFNet [15] by 0.25 dB in PSNR- μ and 0.04 dB in SSIM- μ on Kalantari’s dataset, which represent greater reconstruction performance.

Quantitative Comparison. The visual comparisons on Kalantari’s dataset [13], Tel’s dataset [33] and Hu’s dataset [10] are shown in Fig. 4. We can observe that our

proposed AFUNet achieves more complete scene reconstruction and retains more details. AFUNet demonstrates strong reconstruction capabilities for challenging patches, with a substantial reduction in ghosting artifacts. To assess the generalization capability of the proposed HDR imaging method, we evaluate the model trained on Kalantari’s dataset [13] and tested on Tursun’s dataset [34], which lacks ground truth. Therefore, we only use our human subjective perception to judge the model’s performance in this comparison. The visual comparison on Tursun’s dataset [34] is shown in Fig. 5. We attribute the strong performance to our carefully designed HDR optimization reconstruction algorithm and the unfolding framework. The alignment and fusion sub-problems can complement each other during the reconstruction process. Moreover, cross-iterative alignment and fusion synergy significantly leads to more effective optimization, allowing us to generate high-quality HDR images with improved perceptual quality.

4.3. Ablation Study

To investigate the effectiveness of each key component and the unfolding paradigm for HDR reconstruction, we conducted thorough ablation studies on Kalantari’s dataset [13] using the following variants of our model: (1) **M1**: SFM. (2) **M2**: Adding SAM into M1. (3) **M3**: Adding CFM into M1. (4) **M4**: Adding DCM into M1.

Different Components. We conduct ablation experiments

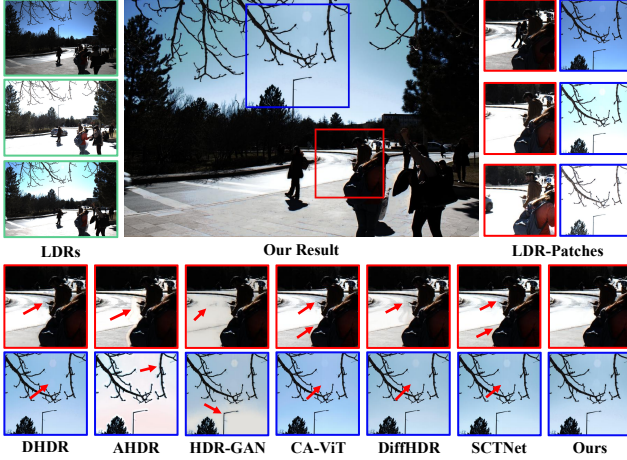


Figure 5. Qualitative comparison between our method and state-of-the-art methods on Tursen’s dataset [34] without ground truth.

Models	SFM	SAM	CFM	DCM	PSNR- μ	PSNR- l	SSIM- μ	SSIM- l
M1	✓				43.94	42.04	0.9917	0.9890
M2	✓	✓			44.48	42.40	0.9918	0.9893
M3	✓		✓		44.62	42.56	0.9921	0.9895
M4	✓			✓	44.45	42.39	0.9919	0.9899
AFUNet	✓	✓	✓	✓	44.91	42.59	0.9923	0.9906

Table 4. Ablation study of different components in the proposed unfolding framework on Kalantari’s dataset [13].

to evaluate the contribution of each component within AFUNet. The experimental cases and corresponding qualitative results are presented in Tab. 4. The results demonstrate the effectiveness of the SAM, CFM, and DCM, with each component contributing to notable improvements in the performance of our method. Specifically, our thorough ablation studies conclusively show the effectiveness and necessity of the alignment module in the M2 cases, showing that incorporating the alignment process into the fusion process can improve the final reconstruction quality.

Different HDR Reconstruction Paradigms. We investigate the effectiveness of our proposed progressive alignment and fusion unfolding paradigm, introducing a novel perspective on analyzing our framework. Each stage of our model consists of two processes: alignment and fusion. As shown in Tab. 5, we can reconstruct the framework into two distinct paradigms. Specifically, we explore the cross-iterative Alignment-Fusion paradigm denoted as “AF”, and the cross-iterative Fusion-Alignment paradigm denoted as “FA” as alternative perspectives for evaluating our unfolding algorithm. As shown in Tab. 5, the “FA” paradigm demonstrates a slight performance decline compared to our “AF” paradigm, highlighting the effectiveness of the alignment process while maintaining competitive quantitative results due to our robust formulation.

Number of Stages. We investigate the impact of different

Models	AF	FA	PSNR- μ	PSNR- l	SSIM- μ	SSIM- l
P1	✓		44.91	42.59	0.9923	0.9906
P2		✓	44.72	42.32	0.9923	0.9904

Table 5. Ablation study of different paradigms. “AF” first conducts alignment followed by fusion, and “FA” first conducts fusion followed by alignment, both in an alternating sequence.

Stages	PSNR- μ	PSNR- l	SSIM- μ	SSIM- l
2	44.40	41.45	0.9918	0.9881
3	44.83	42.62	0.9923	0.9903
4	44.91	42.59	0.9923	0.9906
5	44.85	42.91	0.9923	0.9908
6	44.93	42.84	0.9923	0.9910

Table 6. The impact of different numbers of iterative reconstruction stages in AFUNet on Kalantari’s dataset [13].

numbers of unfolding iterative stages in AFUNet, specifically 2, 3, 4 (default), 5, and 6, to explore their influence on model performance. As shown in Tab. 6, there is a correlation between the number of stages and reconstruction performance, demonstrating the effectiveness of our iterative design. Fewer stages result in lower performance compared to the default configuration but the 3-stage setting surpasses the previous stage-of-the-art method in PSNR- μ and SSIM- μ , showcasing the superior reconstruction ability of our AFUNet. While using 5 and 6 stages yields slight performance improvements over 4 stages, it comes at the cost of increased training time and model complexity. Thus, we select 4 stages as the default setting, striking an optimal balance between performance and model complexity.

5. Conclusion

In this paper, we propose AFUNet, a novel and effective cross-iterative Alignment and Fusion deep Unfolding Network for HDR reconstruction. We first formulate the HDR reconstruction objective, introducing spatial correspondence priors among LDR images. Then, we derive the HDR reconstruction process in detail, which is subsequently unfolded into an end-to-end trainable network. Each iteration consists of two sub-problems—alignment and fusion—where we carefully design corresponding modules to iteratively optimize the overall problem. Extensive experiments show that AFUNet excels in producing realistic HDR images with more detail and less ghosting, outperforming state-of-the-art methods.

Acknowledgments. This work was supported in part by the National Natural Science Foundation of China under Grant 62201387 and in part by the Fundamental Research Funds for the Central Universities.

References

- [1] Luca Bogoni. Extending dynamic range of monochrome and color images through fusion. In *IEEE International Conference on Pattern Recognition*, pages 7–12, 2000. 1
- [2] Sibi Catley-Chandar, Thomas Tanay, Lucas Vandroux, Aleš Leonardis, Gregory Slabaugh, and Eduardo Pérez-Pellitero. FlexHDR: Modeling alignment and exposure uncertainties for flexible HDR imaging. *IEEE Transactions on Image Processing*, 31:5923–5935, 2022. 2, 6
- [3] Jie Chen, Zaifeng Yang, Tsz Nam Chan, Hui Li, Junhui Hou, and Lap-Pui Chau. Attention-guided progressive neural texture fusion for high dynamic range image restoration. *IEEE Transactions on Image Processing*, 31:2661–2672, 2022. 6
- [4] Rufeng Chen, Bolun Zheng, Hua Zhang, Quan Chen, Chenggang Yan, Gregory Slabaugh, and Shanxin Yuan. Improving dynamic HDR imaging with fusion transformer. In *Proceedings of the AAAI Conference on Artificial Intelligence*, pages 340–349, 2023. 2
- [5] Paul E Debevec and Jitendra Malik. Recovering high dynamic range radiance maps from photographs. In *Proceedings of the 24th Annual Conference on Computer Graphics and Interactive Techniques*, pages 369–378, 1997. 1
- [6] Donald Geman and Chengda Yang. Nonlinear image recovery with half-quadratic regularization. *IEEE Transactions on Image Processing*, 4(7):932–946, 1995. 3
- [7] Thorsten Grossch et al. Fast and robust high dynamic range image generation with camera and object movement. *Vision, Modeling and Visualization, RWTH Aachen*, 277284(3):2, 2006. 1
- [8] Zhen Guo and Hongping Gan. CPP-Net: Embracing multi-scale feature fusion into deep unfolding CP-PPA network for compressive sensing. In *Proceedings of the IEEE/CVF Conference on Computer Vision and Pattern Recognition*, pages 25086–25095, 2024. 2
- [9] Wenhui Hong, Hao Zhang, and Jiayi Ma. MERF: a practical HDR-like image generator via mutual-guided learning between multi-exposure registration and fusion. *IEEE Transactions on Image Processing*, 33:2361–2376, 2024. 2
- [10] Jun Hu, Orazio Gallo, Kari Pulli, and Xiaobai Sun. HDR deghosting: How to deal with saturation? In *Proceedings of the IEEE/CVF International Conference on Computer Vision*, pages 1163–1170, 2013. 1, 6, 7
- [11] Tao Hu, Qingsen Yan, Yuankai Qi, and Yanning Zhang. Generating content for HDR deghosting from frequency view. In *Proceedings of the IEEE/CVF Conference on Computer Vision and Pattern Recognition*, pages 25732–25741, 2024. 6, 7
- [12] Yan Huang, Shang Li, Liang Wang, Tieniu Tan, et al. Unfolding the alternating optimization for blind super resolution. *Advances in Neural Information Processing Systems*, 33:5632–5643, 2020. 2
- [13] Nima Khademi Kalantari and Ravi Ramamoorthi. Deep high dynamic range imaging of dynamic scenes. *ACM Transactions on Graphics*, 36(4):1–12, 2017. 2, 6, 7, 8
- [14] Sing Bing Kang, Matthew Uyttendaele, Simon Winder, and Richard Szeliski. High dynamic range video. *ACM Transactions on Graphics*, 22(3):319–325, 2003. 1
- [15] Lingtong Kong, Bo Li, Yike Xiong, Hao Zhang, Hong Gu, and Jinwei Chen. SAFNet: Selective alignment fusion network for efficient HDR imaging. In *Proceedings of the European Conference on Computer Vision*, 2024. 2, 6, 7
- [16] Chul Lee, Yuelong Li, and Vishal Monga. Ghost-free high dynamic range imaging via rank minimization. *IEEE Signal Processing Letters*, 21(9):1045–1049, 2014. 1
- [17] Keuntek Lee, Jaehyun Park, Gu Yong Park, and Nam Ik Cho. RFG-HDR: Representative feature-guided transformer for multi-exposure high dynamic range imaging. In *2024 IEEE International Conference on Image Processing*, pages 1521–1527. IEEE, 2024. 6
- [18] Zhen Liu, Wenjie Lin, Xinpeng Li, Qing Rao, Ting Jiang, Mingyan Han, Haoqiang Fan, Jian Sun, and Shuaicheng Liu. ADNet: Attention-guided deformable convolutional network for high dynamic range imaging. In *Proceedings of the IEEE/CVF Conference on Computer Vision and Pattern Recognition*, pages 463–470, 2021. 2, 6
- [19] Ze Liu, Yutong Lin, Yue Cao, Han Hu, Yixuan Wei, Zheng Zhang, Stephen Lin, and Baining Guo. Swin transformer: Hierarchical vision transformer using shifted windows. In *Proceedings of the IEEE/CVF International Conference on Computer Vision*, pages 10012–10022, 2021. 5
- [20] Zhen Liu, Yinglong Wang, Bing Zeng, and Shuaicheng Liu. Ghost-free high dynamic range imaging with context-aware transformer. In *Proceedings of the European Conference on Computer Vision*, pages 344–360, 2022. 2, 6, 7
- [21] Kede Ma, Hui Li, Hongwei Yong, Zhou Wang, Deyu Meng, and Lei Zhang. Robust multi-exposure image fusion: a structural patch decomposition approach. *IEEE Transactions on Image Processing*, 26(5):2519–2532, 2017. 1
- [22] Kede Ma, Zhengfang Duanmu, Hanwei Zhu, Yuming Fang, and Zhou Wang. Deep guided learning for fast multi-exposure image fusion. *IEEE Transactions on Image Processing*, 29:2808–2819, 2020. 1
- [23] Truong Thanh Nhat Mai, Edmund Y Lam, and Chul Lee. Deep unrolled low-rank tensor completion for high dynamic range imaging. *IEEE Transactions on Image Processing*, 31:5774–5787, 2022. 2
- [24] Rafał Mantiuk, Kil Joong Kim, Allan G Rempel, and Wolfgang Heidrich. HDR-VDP-2: A calibrated visual metric for visibility and quality predictions in all luminance conditions. *ACM Transactions on graphics*, 30(4):1–14, 2011. 6
- [25] Ge Meng, Jingjia Huang, Yingying Wang, Zhenqi Fu, Xinghao Ding, and Yue Huang. Progressive high-frequency reconstruction for pan-sharpening with implicit neural representation. In *Proceedings of the AAAI Conference on Artificial Intelligence*, pages 4189–4197, 2024. 2
- [26] Yuzhen Niu, Jianbin Wu, Wenxi Liu, Wenzhong Guo, and Rynson WH Lau. HDR-GAN: HDR image reconstruction from multi-exposed LDR images with large motions. *IEEE Transactions on Image Processing*, 30:3885–3896, 2021. 6
- [27] Tae-Hyun Oh, Joon-Young Lee, Yu-Wing Tai, and In So Kweon. Robust high dynamic range imaging by rank minimization. *IEEE Transactions on Pattern Analysis and Machine Intelligence*, 37(6):1219–1232, 2014. 1

- [28] K. Ram Prabhakar, V. Sai Srikanth, and R. Venkatesh Babu. DeepFuse: A deep unsupervised approach for exposure fusion with extreme exposure image pairs. In *Proceedings of the IEEE International Conference on Computer Vision*, 2017. 1
- [29] Pradeep Sen, Nima Khademi Kalantari, Maziar Yaezoubi, Soheil Darabi, Dan B Goldman, and Eli Shechtman. Robust patch-based HDR reconstruction of dynamic scenes. *ACM Transactions on Graphics*, 31(6):203, 2012. 1
- [30] K. Simonyan and A. Zisserman. Very deep convolutional networks for large-scale image recognition. In *International Conference on Learning Representations*, 2015. 6
- [31] Jiechong Song, Bin Chen, and Jian Zhang. Dynamic path-controllable deep unfolding network for compressive sensing. *IEEE Transactions on Image Processing*, 32:2202–2214, 2023. 2
- [32] Jou Won Song, Ye-In Park, Kyeongbo Kong, Jaeho Kwak, and Suk-Ju Kang. Selective TransHDR: Transformer-based selective HDR imaging using ghost region mask. In *European Conference on Computer Vision*, pages 288–304. Springer, 2022. 2
- [33] Steven Tel, Zongwei Wu, Yulun Zhang, Barthélémy Heyrman, Cédric Demonceaux, Radu Timofte, and Dominique Ginghac. Alignment-free HDR deghosting with semantics consistent transformer. In *Proceedings of the IEEE/CVF International Conference on Computer Vision*, pages 12836–12845, 2023. 2, 6, 7
- [34] Okan Tarhan Tursun, Ahmet Oğuz Akyüz, Aykut Erdem, and Erkut Erdem. An objective deghosting quality metric for HDR images. In *Computer Graphics Forum*, pages 139–152, 2016. 6, 7, 8
- [35] Chong Wang, Lanqing Guo, Yufei Wang, Hao Cheng, Yi Yu, and Bihang Wen. Progressive divide-and-conquer via subsampling decomposition for accelerated mri. In *Proceedings of the IEEE/CVF Conference on Computer Vision and Pattern Recognition*, pages 25128–25137, 2024. 2
- [36] Hebaixu Wang, Meiqi Gong, Xiaoguang Mei, Hao Zhang, and Jiayi Ma. Deep unfolded network with intrinsic supervision for pan-sharpening. In *Proceedings of the AAAI Conference on Artificial Intelligence*, pages 5419–5426, 2024. 2
- [37] Zhou Wang, Alan C Bovik, Hamid R Sheikh, and Eero P Simoncelli. Image quality assessment: from error visibility to structural similarity. *IEEE transactions on image processing*, 13(4):600–612, 2004. 6
- [38] Shangzhe Wu, Xu Jiarui, Tai Yu-Wing, and Tang Chi-Keung. Deep high dynamic range imaging with large foreground motions. In *Proceedings of the European Conference on Computer Vision*, pages 117–132, 2018. 6
- [39] Qingsen Yan, Dong Gong, Qinfeng Shi, Anton van den Hengel, Chunhua Shen, Ian Reid, and Yanning Zhang. Attention-guided network for ghost-free high dynamic range imaging. In *Proceedings of the IEEE/CVF Conference on Computer Vision and Pattern Recognition*, pages 1751–1760, 2019. 2, 6
- [40] Qingsen Yan, Lei Zhang, Yu Liu, Yu Zhu, Jinqiu Sun, Qinfeng Shi, and Yanning Zhang. Deep HDR imaging via a non-local network. *IEEE Transactions on Image Processing*, 29:4308–4322, 2020. 2, 6
- [41] Qingsen Yan, Weiye Chen, Song Zhang, Yu Zhu, Jinqiu Sun, and Yanning Zhang. A unified HDR imaging method with pixel and patch level. In *Proceedings of the IEEE/CVF Conference on Computer Vision and Pattern Recognition*, pages 22211–22220, 2023. 2, 6
- [42] Qingsen Yan, Tao Hu, Yuan Sun, Hao Tang, Yu Zhu, Wei Dong, Luc Van Gool, and Yanning Zhang. Towards high-quality HDR deghosting with conditional diffusion models. *IEEE Transactions on Circuits and Systems for Video Technology*, 2023. 6
- [43] Gang Yang, Man Zhou, Keyu Yan, Aiping Liu, Xueyang Fu, and Fan Wang. Memory-augmented deep conditional unfolding network for pan-sharpening. In *Proceedings of the IEEE/CVF conference on computer vision and pattern recognition*, pages 1788–1797, 2022. 2
- [44] Qian Ye, Jun Xiao, Kin-man Lam, and Takayuki Okatani. Progressive and selective fusion network for high dynamic range imaging. In *Proceedings of the 29th ACM International Conference on Multimedia*, pages 5290–5297, 2021. 2
- [45] Syed Waqas Zamir, Aditya Arora, Salman Khan, Munawar Hayat, Fahad Shahbaz Khan, and Ming-Hsuan Yang. Restormer: Efficient transformer for high-resolution image restoration. In *Proceedings of the IEEE/CVF conference on computer vision and pattern recognition*, pages 5728–5739, 2022. 5
- [46] Kai Zhang, Luc Van Gool, and Radu Timofte. Deep unfolding network for image super-resolution. In *Proceedings of the IEEE/CVF Conference on Computer Vision and Pattern Recognition*, pages 3217–3226, 2020. 2
- [47] Wei Zhang and Wai-Kuen Cham. Gradient-directed multiexposure composition. *IEEE Transactions on Image Processing*, 21(4):2318–2323, 2011. 1
- [48] Xiang Zhang, Genggeng Chen, Tao Hu, Kangzhen Yang, Fan Zhang, and Qingsen Yan. Hi-hdr: Multi-exposure high dynamic range reconstruction with high-low frequency decomposition. In *2024 International Joint Conference on Neural Networks*, pages 1–9. IEEE, 2024. 2
- [49] Man Zhou, Keyu Yan, Jinshan Pan, Wensi Ren, Qi Xie, and Xiangyong Cao. Memory-augmented deep unfolding network for guided image super-resolution. *International Journal of Computer Vision*, 131(1):215–242, 2023. 2
- [50] Henning Zimmer, Andrés Bruhn, and Joachim Weickert. Freehand HDR imaging of moving scenes with simultaneous resolution enhancement. In *Computer Graphics Forum*, pages 405–414, 2011. 1